Fabrication and Molecular Transport Studies of Highly c-Oriented AFI Membranes

Fabrication and Molecular Transport Studies of Highly c-Oriented AFI Membranes

Yang Liu, Bing Zhang, Defei Liu, Ping Sheng, Zhiping Lai

www.elsevier.com/locate/memsci

PII: S0376-7388(16)31781-1
DOI: http://dx.doi.org/10.1016/j.memsci.2017.01.012
Reference: MEMSCI15003

To appear in: *Journal of Membrane Science*

Received date: 28 September 2016
Revised date: 18 December 2016
Accepted date: 7 January 2017

Cite this article as: Yang Liu, Bing Zhang, Defei Liu, Ping Sheng and Zhiping Lai, Fabrication and Molecular Transport Studies of Highly c-Oriented AFI Membranes, *Journal of Membrane Science* http://dx.doi.org/10.1016/j.memsci.2017.01.012

Fabrication and Molecular Transport Studies of Highly c-Oriented AFI Membranes

Yang Liu[a], Bing Zhang[b], Defei Liu[a], Ping Sheng[b*], Zhiping Lai[a*]

[a]Advanced Membranes and Porous Materials Center, Chemical and Biological Engineering, Division of Physical Science and Engineering, King Abdullah University of Science and Technology, Thuwal, KSA

[b]Department of Physics, Hong Kong University of Science and Technology, Clear Water Bay, Kowloon, Hong Kong

zhiping.lai@kaust.edu.sa (Prof. Zhiping Lai)

sheng@ust.hk (Prof. Ping Sheng)

[*]Corresponding authors:

ABSTRACT:

The AFI membrane with one-dimensional straight channels is an ideal platform for various applications. In this work, we report the fabrication of a highly c-oriented, compact and stable AFI membrane by epitaxial growth from an almost close-packed and c-oriented monolayer of plate-like seeds that is manually assembled on a porous alumina support. The straight channels in the membrane are not only aligned vertically along the membrane depth, but are also continuous without disruption. The transport resistance is thus minimized and as a result, the membrane shows almost two orders of magnitude greater permeance in pervaporation of hydrocarbons compared to reported values in the literature. The selectivity of p-xylene to 1,3,5-triisopropylbenzene (TIPB) is approximately 850. In addition, through gas permeation studies on a number of gas and liquid molecules, different transport mechanisms including activated Knudsen diffusion, surface diffusion and molecular sieving were discovered for different diffusion species. The ratio of kinetic diameter to channel diameter, d_m/d_c, and the ratio of the

Lennard-Jones length constant to channel diameter, σ_m/d_c, are found very useful in explaining the different transport behaviors. These results should be useful not only for potential industrial applications of the AFI membranes but also for the fundamental understanding of transport in nanoporous structures.

Keywords: AFI, Zeolite Membrane; Transport Mechanism, Nanopores

1. Introduction

Zeolite membranes have been studied intensively over the last 30 years [1, 2]. Due to their well-defined and highly stable porous structure, zeolite membranes are able to achieve sharp molecular sieving with high transport rates and thus have shown excellent performance in many challenging separation systems such as dehydration [3, 4], CO_2 capture [5, 6], and hydrocarbon mixtures with close-boiling points [7, 8]. However, it is still a considerable challenge to synthesize defect-free membranes over large areas with controllable microstructures. AFI is an important aluminophosphate type of zeolite whose porous structure contains one-dimensional circular channels along the c-axis with a pore size of 0.73 × 0.73 nm [9]. It has two isomorphic forms: $AlPO_4$-5 is a pure aluminophosphate form, while SAPO-5 contains a small amount of silicon in the framework. AFI is resistant to acid, base and organic solvents. It is thermally stable up to 1000 °C. Its unique straight channels and medium range pore size allow not only fast diffusion of molecules compared to other zeolites' 3D pore networks [10] but also embedding of many types of functional guest molecules, which makes the AFI framework a good crystalline host for many host-guest applications such as nonlinear optics [11, 12], light harvesting [13], superconductivity [14], and chemical sensing [15]. AFI has also been studied intensively in catalysis for conversion of hydrocarbons [16], such as for butane or heptane isomerization [17, 18], conversion of benzyl alcohol [19], and toluene alkylation [20]. However, the one-

dimensional porous structure of AFI also imposes a major challenge in membrane fabrication, that is, the membrane should be c-oriented so that the straight channels are aligned along the membrane depth to allow efficient transport. In the past decades, there have been many attempts to fabricate c-oriented AFI membranes on different supports using various methods [21, 22]. Girnus et al. reported vertically aligned $AlPO_4$-5-in-nickel membranes generated using rod-shaped crystals with microwave heating [23]. Karanikolos et al. prepared c-oriented $AlPO_4$-5 films by tertiary growth on seeded silicon substrates [24]. Yang et al. fabricated SAPO-5 membranes on porous α-Al_2O_3 substrates by using in-situ crystallization and microwave heating, but the orientation was random [25]. Stoeger et al. synthesized c-oriented CoSAPO-5 membranes by microwave enhanced growth on TiO_2-coated porous alumina [26]. We have also reported the synthesis of highly c-oriented AFI membranes on nonporous aluminum substrates [27]. However, in all of these reports either there is no gas permeation data, or the membrane was grown from random oriented seeds so even though the membrane was c-oriented due to competitive growth, its orientation changed gradually along the membrane thickness and therefore disturbed the transport along the straight channels [28].

Herein we report the successful fabrication of highly c-oriented, compact and mechanically stable AFI membranes on porous α-Al_2O_3 substrates through epitaxial growth of micrometer sized, plate-like and c-oriented seed layers. The high membrane quality and the optimized microstructure not only showed orders of magnitude improvement in membrane permeance and selectivity but also allowed us to investigate the intrinsic transport properties using gas permeation and liquid pervaporation tests. Different transport mechanisms, including Knudsen diffusion, surface diffusion and sharp molecular sieving, were discovered for different molecules.

These results should be useful not only for potential industrial applications of the AFI membranes but also for the fundamental understanding of the transport in nanoporous structures.

2. Experimental

2.1 Materials

The AFI membrane fabrication involved the following chemicals: pseudoboehmite (Catapal A, Sasol), phosphoric acid (H_3PO_4, 85%, Panreac), silica gel (40 wt%, Ludox HS-40, Sigma-Aldrich) trimethylamine (TEA, 99.5%, Sigma-Aldrich), 3-chloropropyl trimethoxysilane (3CP-TMS, Sigma-Aldrich), anhydrous toluene (99.8%, Sigma-Aldrich), polyvinyl alcohol (PVA, 98-99%, Mw=146,000-186,000, Sigma-Aldrich) and aluminum isopropoxide (AIP, 98%, Acros). N-heptane, xylene isomers, mesitylene and 1,3,5-triisopropylbenzene (TIPB) were all HPLC grade and obtained from Sigma-Aldrich. All chemicals were used as received without further treatments.

2.2. Synthesis of plate-like SAPO-5 seeds

Plate-like SAPO-5 seeds were synthesized from a precursor solution with a molar composition of 1 Al_2O_3: 0.8 P_2O_5: 1 SiO_2: 3.5 TEA: 50 H_2O that was prepared as follows. 5.68 g H_3PO_4, 22.8 g deionized (DI) water and 4.42 g pseudoboehmite were mixed subsequently and stirred for 4 h. 4.62 g silica gel was then added to the above solution to form a slurry and stirred for 1 h. Next, 10.82 g TEA was added to the slurry using a dropping funnel. Finally, after rigorous stirring for 14 h, the slurry was loaded into a microwave oven (CEM Mars 5), heated to 180 °C within 1.5 minutes, and then incubated for 2 h. After that, the resulting crystals were washed, collected by centrifugation, dried at 120 °C overnight, and then stored for later use. The as-synthesized plate-like SAPO-5 crystals that had a large flat (001) face were used as seeds.

2.3. Assembly of SAPO-5 seeds on α-Al_2O_3 disks

To enhance the interaction between seeds and the porous α-alumina substrate, seeds were functionalized with a silane coupling agent, 3CP-TMS, while the substrate was coated with a PVA layer (Fig. 1a). Specifically, 1 g dry SAPO-5 seeds were added to a mixture of 5 ml 3CP-TMS and 40 ml anhydrous toluene in a glove box. The mixture was heated to 110 °C and refluxed overnight under argon protection. Afterwards, the functionalized seeds were washed with anhydrous toluene 3 times to remove extra 3CP-TMS and then dried at 120 °C. The polished α-Al_2O_3 substrate (2.2 cm in diameter) was coated with a layer of PVA by a simple slip coating process from an 8 wt% PVA aqueous solution and dried at 80 °C. The functionalized SAPO-5 seeds were assembled on the PVA-coated substrate using a manual rubbing method, which was first developed for the synthesis of *b*-oriented MFI membranes [7, 29]. Due to the plate-like shape, seeds naturally attach their (001) face to the substrate and therefore form a c-oriented seed layer (Fig. 1b). The quality of the seed layer was inspected with a high resolution optical microscope (VHX-600, Keyence). The seeded substrate was placed on a hotplate to melt the PVA. After cooling, the extra seeds were removed by ultrasonication. Finally, the seeded substrate was calcined at 800 °C for 6 h with a heating rate of 0.2 ^{o}C/min and a cooling rate of 0.5 ^{o}C/min to remove the PVA layer and then the seed layer was subjected to a secondary growth process where seeds became larger by epitaxial growth to close the interstitial gaps.

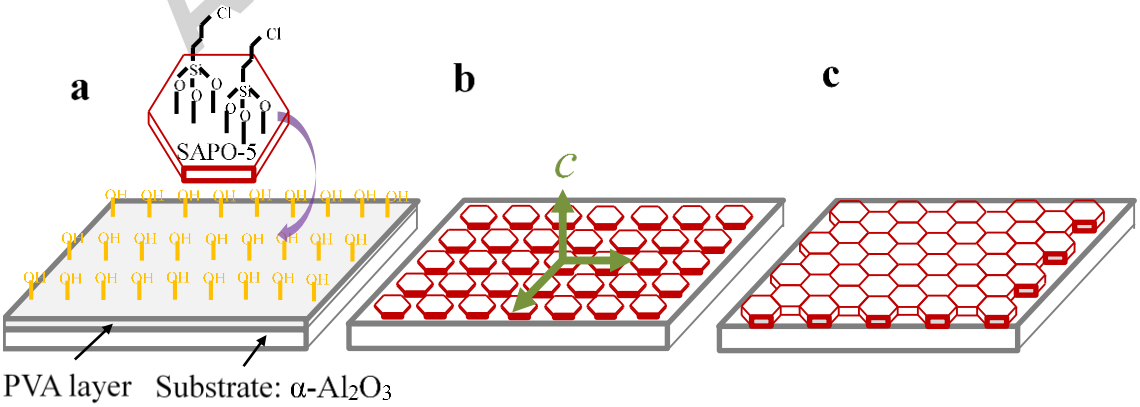

Fig. 1. Schematic illustration of the AFI membrane fabrication procedure: (a) Functionalization of the plate-like SAPO-5 seeds using 3CP-TMS and surface modification of the α-Al_2O_3 substrate by a PVA layer; (b) Formation of a highly c-oriented seed monolayer on a flat α-Al_2O_3 substrate by a manual rubbing method; (c) Secondary growth of the seed layer to form a continuous c-oriented AFI membrane.

2.4. Secondary growth

The secondary growth was executed by a hydrothermal method. The growth solution with a molar composition of 1 Al_2O_3: 1.3 P_2O_5: 0.8 TEA: 160 H_2O was prepared as follows. 5 g AIP was added to 34.28 g DI water and stirred for 5 h. Then, 2.13 ml H_3PO_4 was added dropwise and stirred for 1 h. Subsequently, 1.35 ml TEA was added dropwise. After stirring for 12 h, the mixture was transferred to a Teflon-lined stainless steel autoclave. The seeded α-Al_2O_3 substrate was immersed vertically inside the growth solution with the aid of a Teflon holder. The autoclave was placed in a preheated oven (150 °C) for 24 h and then quenched to room temperature by tap-water. The final result was a compact and highly c-oriented AFI membrane, as shown in Fig. 1c. The membrane was washed, dried and calcined at 540 °C for 4 h in open air with heating and cooling rates of 1 °C/min.

2.5. Characterization of the AFI membrane

Scanning electron micrographs (SEM) were obtained with a Quanta 200 or Quanta 600 microscope. X-ray diffraction (XRD) was performed on a Bruker D8 Advance Diffractometer. Single-gas permeation tests, including hydrogen, helium, nitrogen, methane, argon, carbon dioxide, ethylene, ethane, propylene, *n*-butane and *i*-butane were performed at room temperature by a custom-designed steady-state permeation setup, as shown in Fig. 2. The membrane was placed in a stainless steel permeation cell with the AFI layer facing the feed side and then sealed

on both sides with O-rings. The permeation area (A) of the membrane was 2.34×10^{-4} m^2. The feed pressure was varied between 1 atm and 5 atms. The permeate side was connected to a bubble flow meter at atmospheric pressure.

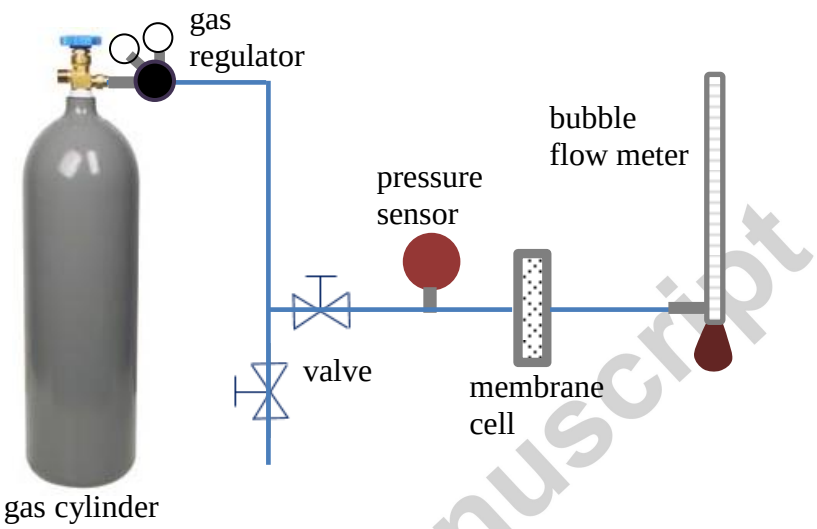

Fig. 2. Schematic diagram of the steady-state permeation setup.

The gas permeance was calculated from the permeation flux divided by the transmembrane pressure drop for gases, using the following equation,

$$P = \frac{J}{\Delta p} = \frac{pV}{RTA}\frac{1}{p^F - p^P} \quad (1)$$

where P is the permeance, J is the permeation flux, $\Delta p = p^F - p^P$ is the transmembrane pressure drop (TMP) between the feed pressure p^F and the permeate pressure p^P, p is the atmosphere pressure, V is the volume flowrate measured by the bubble meter, R is the ideal gas constant, T is the permeation temperature, and A is the permeation area of the membrane.

Single-component pervaporation tests were performed using a pervaporation setup, as shown in Fig. 3. The liquid was kept at 1 atm, while the permeate side was first connected to a liquid nitrogen cold trap and then a mechanical pump (XDS-5, Edwards). The vacuum degree was measured by a vacuum pressure gauge. The membrane was activated/reactivated under vacuum

for 6 h at 100 °C before each measurement. The cold trap was cleaned, dried, weighed and connected to the setup in sequence.

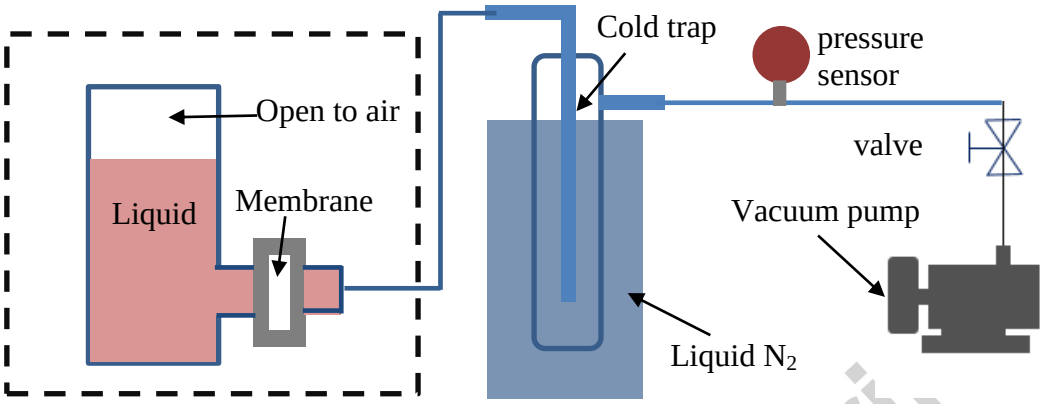

Fig. 3. Schematic representation of the pervaporation setup.

The permeation flux was determined based on the amount of liquid collected in the cold trap under a certain time period. The permeance was calculated from the permeation flux divided by the fugacity difference (saturated vapor pressure minus the permeate pressure) for pervaporation, using the following equation:

$$P = \frac{J}{\Delta p} = \frac{Q}{MAt}\frac{1}{p^{sat}-p^{P}} \quad (2)$$

where P is the permeance, J is the permeation flux, $\Delta p = p^{sat} - p^{P}$ is the fugacity difference between the saturated vapor pressure p^{sat} and the permeate pressure p^{P}, Q is the liquid amount collected in the cold trap under a certain time period t, M is the molecular weight of the measuring liquid, and A is the permeation area of the membrane.

3. Results and discussion

3.1 Synthesis of plate-like SAPO-5 seeds

Ideally, the crystal morphology of seeds should have a large lateral to thickness aspect ratio to induce formation of a plate-like shape, as illustrated in Fig. 1a. It helps to form a thin monolayer of c-oriented seeds. Unfortunately, most reported AFI crystals typically exhibit an

elongated hexagonal rod shape under normal synthesis conditions. Jhung et al. first reported that under fast microwave heating conditions, SAPO-5 crystals could form the desired plate-like shape [30]. In this work we further optimized the crystallization conditions. It was found that the SAPO-5 crystal morphology was particularly sensitive to the heating rate, synthesis temperature and synthesis time as shown in Fig. 4a-d where these parameters were changed slightly. Finally, the crystals obtained under the synthesis conditions of those shown in Fig. 4a, which have a plate-like hexagonal shape with a thickness of 2 μm and a diameter of 6 μm, were identified to be the best in terms of the aspect ratio, the crystallinity and the size uniformity.

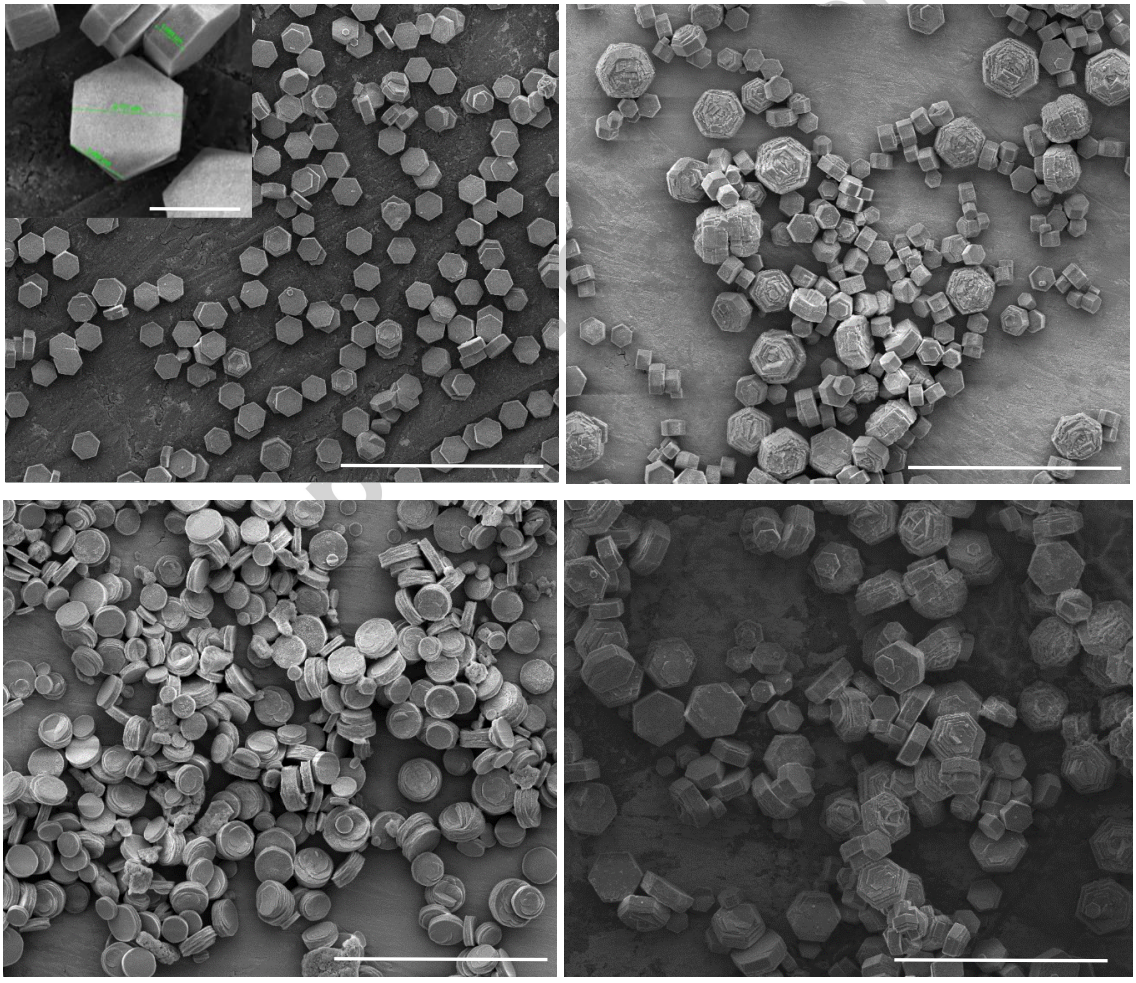

Fig. 4. SAPO-5 crystals synthesized by microwave heating at different heating rates, temperatures and durations: (a) AFI crystals obtained by heating to 180 °C within 1.5 minutes

and holding for 2 h; (b) heating to 185 °C within 1.5 minutes and holding for 2 h; (c) heating to 180 °C within 2 minutes and holding for 2 h; (d) heating to 180 °C within 1.5 minutes and holding for 2.2 h.

3.2. Manual assembly of SAPO-5 crystals on porous α-Al_2O_3 support

Yoon and co-workers [31, 32] developed a very simple rubbing method to assemble zeolite particles into a dense packed monolayer on flat surfaces. This method works very well with zeolite A and MFI crystals, but was found less effective with SAPO-5 crystals. The reason is due to weak interactions between the seeds and the substrate surface. Hence firstly, the SAPO-5 seed was functionalized with a silane coupling agent, 3CP-TMS, and the substrate was coated with a PVA layer to enhance the interaction. After such treatments the coverage was significantly improved as shown in Fig. 5. Since the crystal size is large enough, the seed layer can be inspected with a high resolution optical microscope to ensure that there are no large void areas. After inspection, the samples can be used directly for membrane growth. From Fig. 5b, it is evident that a monolayer is formed with almost all seeds attaching their flat (001) surface to the support and hence the seed layer should be highly c-oriented, as verified by the XRD pattern in Fig. 7A.

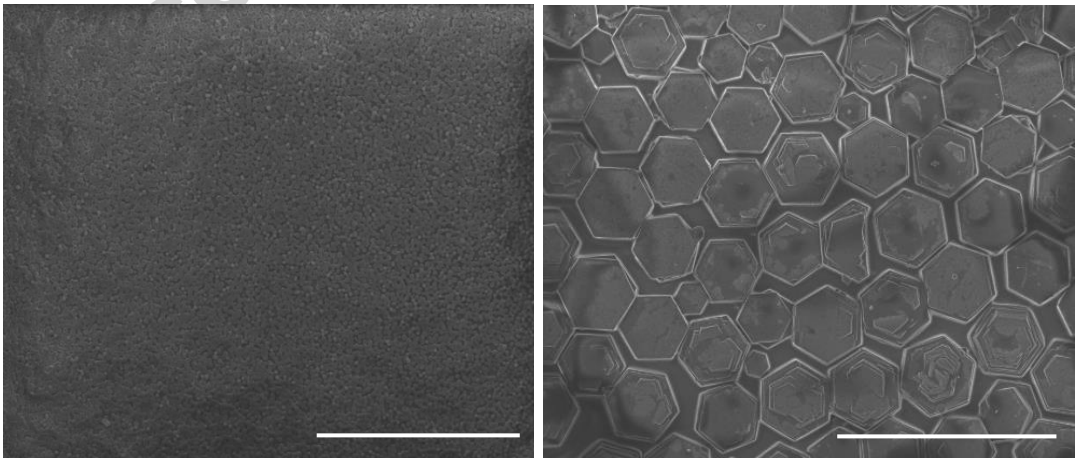

Fig. 5. SAPO-5 seed layer coated on a porous α-Al_2O_3 substrate by a manual rubbing method: (a) at low resolution; (b) at high resolution.

3.3. Growth of highly c-oriented AFI membranes

Fig. 6 and Fig. 7 show the SEM images for the membranes at different stages from 3 h to 24 h. During the first three hours, it can be seen that intensive nucleation occurs on the top surface (Fig. 6a). After six hours, intensive growth along the side surfaces is also evident (Fig. 6b). The lattice mismatch between the seed layer (SAPO-5) and the secondary growth layer ($AlPO_4$-5) is considered to be negligible since these two forms of AFI zeolite are isomorphic. After growth for 12 h (Fig. 6c), most gaps were closed due to growth of the seed crystals. A close look at the newly formed crystals inside the gap (Fig. 6d) revealed that almost all the newly formed crystals had their edges aligned with each other, indicating that these crystals were not formed randomly but rather induced from the seed crystals, and hence the growth was epitaxial. This is desirable not only for retaining the membrane orientation but also for maintaining the straight channels.

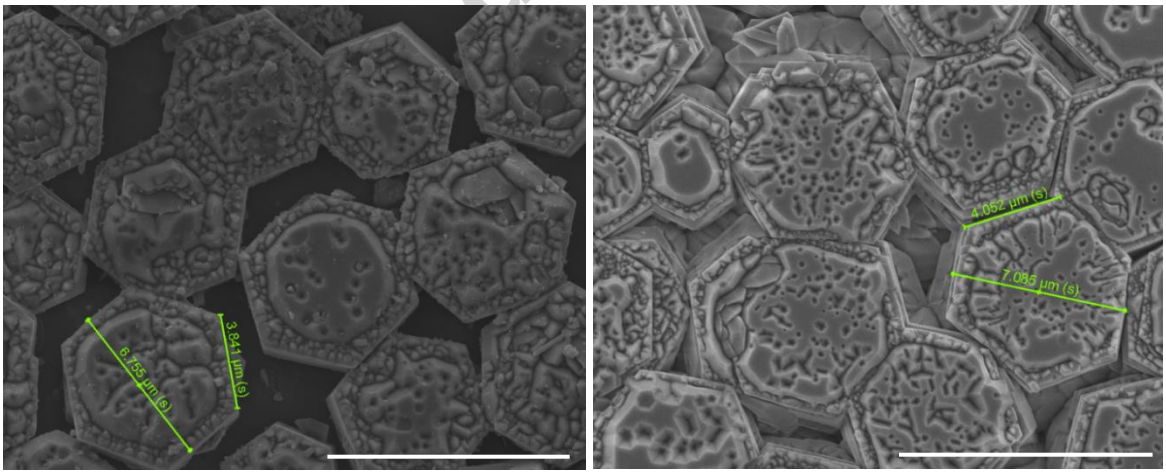

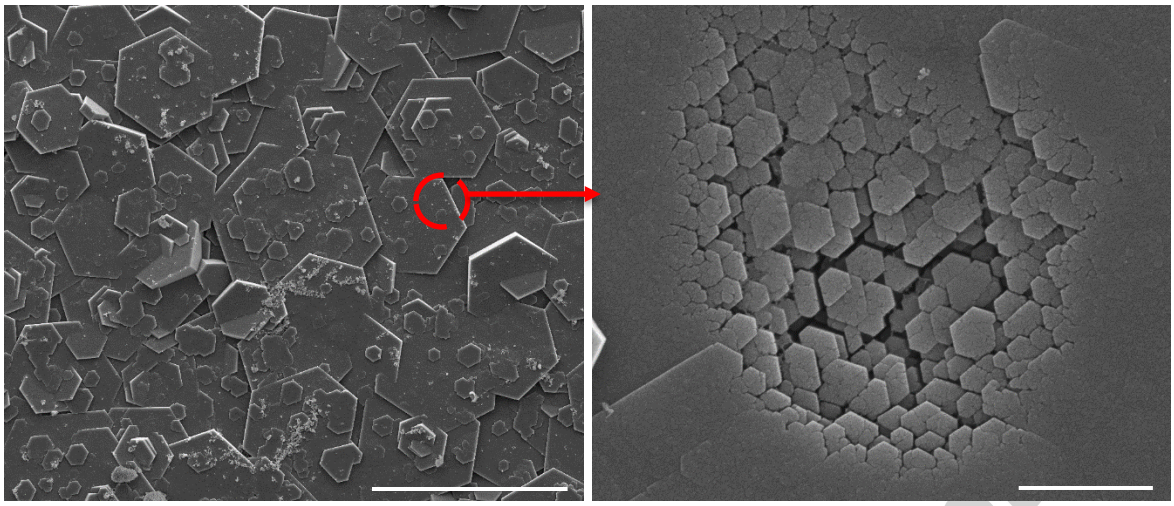

Fig. 6. SEM images for the AFI membrane at different growth times: (a) 3 h; (b) 6 h; (c) 12 h; (d) a high resolution image of an incomplete growth area at 12 h.

After 24 h of growth, as shown in Fig. 7a and Fig. 7b, a continuous AFI membrane was successfully obtained with its c-orientation well retained. The membrane layer inter-grew into the porous α-Al_2O_3 substrate and formed a stable AFI membrane with a thickness of approximately 10 μm, as shown in Fig. 7c. Fig. 7d shows the XRD patterns of the seed layer and the membranes after 6 h and 24 h growth. All three patterns have a strong (002) peak, which confirms the seed layer is highly c-oriented and the membrane kept the c-orientation during the whole growth procedure.

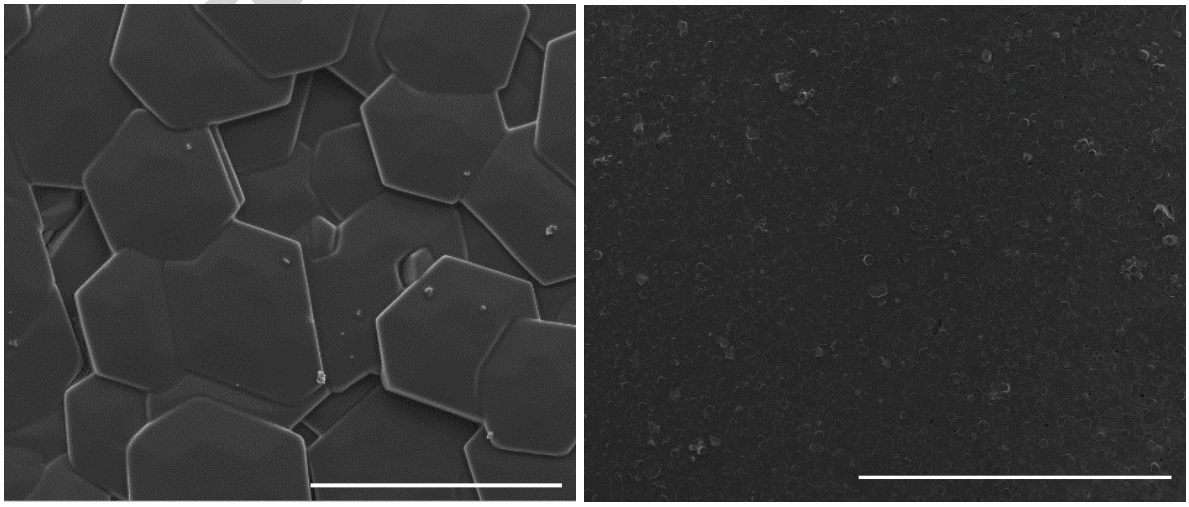

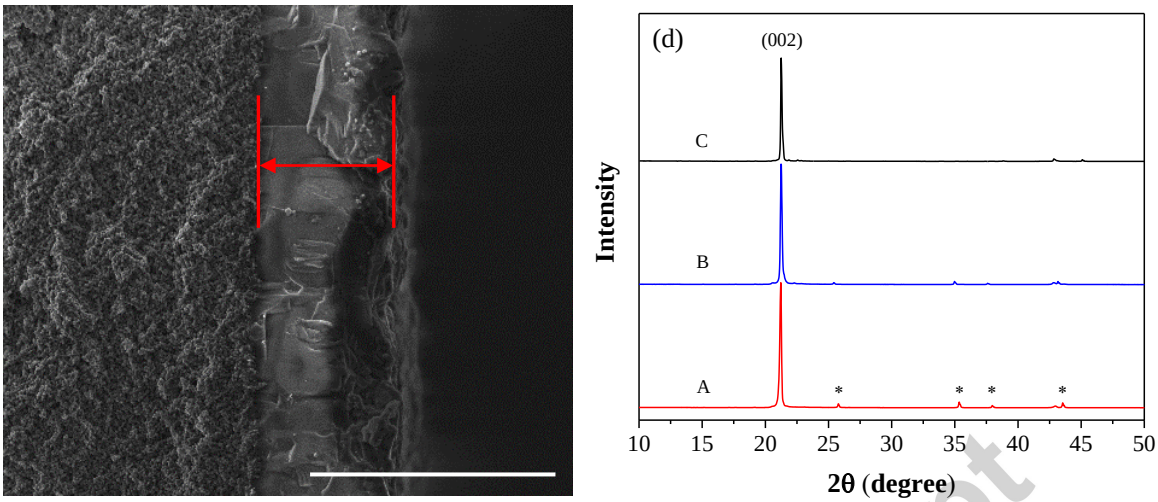

Fig. 7. Characterization of the AFI membrane after 24 h of growth: (a) Top surface in high magnification; (b) top surface in low magnification; (c) cross-section of AFI membrane; (d) XRD patterns of the membrane at different growth stages: (A) seeds layer, (B) 6 h and (D) 24 h. The asterisks mark the peaks for the α-Al_2O_3 substrate.

3.4. Gas permeation and pervaporation tests

The single-gas permeation results for six different gases, H_2, He, CH_4, N_2, Ar and CO_2 are plotted in Fig. 8. Fig. 8a shows that all the gas permeance values are independent of the mean trans-membrane pressure $(p^F+p^P)/2$, where p^F is the feed pressure and p^P is the permeate pressure. Fig. 8b shows that the gas permeance is inversely proportional to the squared root of the gas molecular weight $(1/M)^{1/2}$. These relationships suggest that the fabricated AFI membrane contains a negligible amount of microporous defects and the gas transport mechanism is Knudsen diffusion. The gas permeance values of the AFI membrane are comparable to those of the ZIF-68 membrane which has a similar pore size (7.5 Å) and straight 1D channels [33] after normalizing with the membrane thickness.

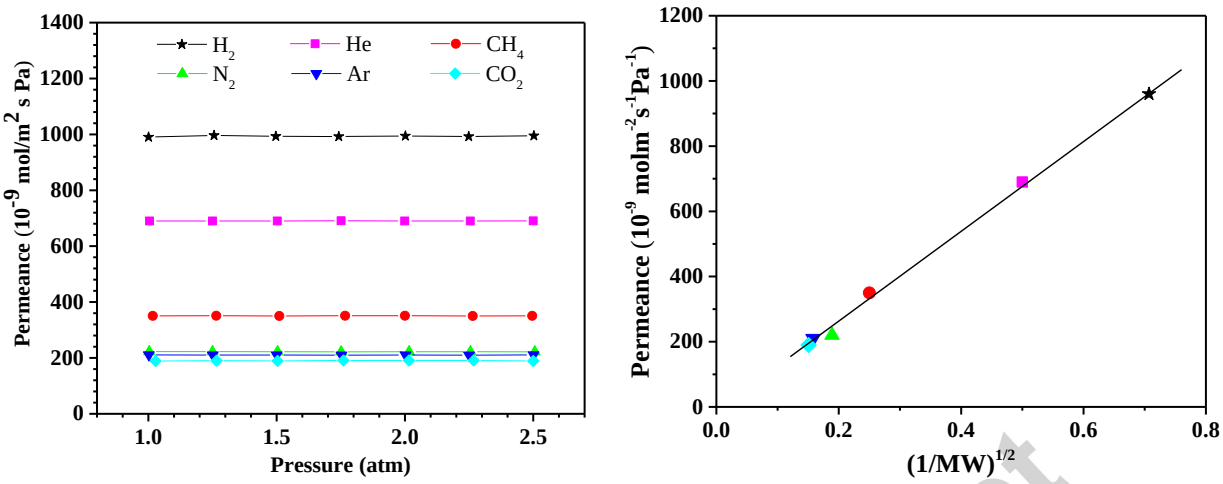

Fig. 8. (a) Gas permeance in the AFI membrane at different mean transmembrane pressures $(p^F+p^P)/2$, where p^F is the feed pressure and p^P is the permeate pressure; (b) relationship between gas permeance and the square root of gas molecular weight.

The following equation based on the activated Knudsen diffusion model or gas-translational model [34, 35] was thus used to estimate the gas permeance through AFI channels:

$$P = \frac{\varepsilon d}{3\tau L}\sqrt{\frac{8}{\pi MRT}}\exp\left(-\frac{E_a}{RT}\right) \quad (3)$$

where d is the membrane pore size equal to 0.73 nm, ε is the areal porosity equal to 0.256 calculated from the geometry of the AFI unit cell, τ is the tortuosity (which should be 1 here) for one dimensional channels, L is the membrane thickness equal to 10 μm, R is the gas constant, T is the operation temperature, M is the molecular weight, and Ea is the activation energy to overcome the diffusion barrier. Without considering the activation energy term, the estimated permeance values for He, H_2, N_2, CH_4, Ar and CO_2 are 3.2×10^{-6}, 4.5×10^{-6}, 1.2×10^{-6}, 1.6×10^{-6}, 1.0×10^{-6} and 9.6×10^{-7} mol/m^2 s Pa, respectively, which are approximately 4.5~5.5 times higher than the experimental values shown in Fig. 8. Therefore, the activation energy for diffusion is approximately 3.7~4.2 kJ/mol.

Fig. 9 shows the pervaporation permeance at room temperature for several hydrocarbons (n-heptane, xylene isomers, mesitylene and 1,3,5-triisopropylbenzene) that have various kinetic diameters. These kinetic diameters as well as other physical properties are listed in Table 1. It was found that for molecules smaller than the pore size, the permeance decreases slightly with the kinetic diameter. It is noted that mesitylene (7.5 Å) is slightly larger than the channel size (7.3 Å), yet it can pass through the AFI channels quickly. Similar observations have also reported in many other zeolite systems that the effective pore size of zeolites is often found larger than the crystallographic pore size and the deviation sometimes can be up to 0.5 Å [36-39]. However, for molecules significantly larger than the pore size, such as TIPB (kinetic diameter 8.5 Å), the permeance drops by more than two orders of magnitude due to the sharp molecular sieving effect, giving a *p*-xylene to TIPB selectivity of approximately 850. The high selectivity indicates the high quality of the membrane. Additionally, the permeance of n-heptane is approximately 3.2×10^{-5} mol/m^2·s·Pa, and this value is almost two orders of magnitude higher compared to literature reported results. For examples, a value of 7.3×10^{-7} mol/m^2·s·Pa was reported for a 1.5 μm thick c-oriented SAPO-5 membrane [21]; and a value of 2.0×10^{-7} mol/m^2·s·Pa was reported for a 5 μm thick randomly oriented SAPO-5 membrane [25]. If the membrane thickness here is considered to be 10 μm, the membrane permeability will be even higher. Such a significant improvement clearly shows the advantage of the optimum membrane microstructure achieved by our novel membrane synthesis procedure, that is, the straight channels are not only well aligned but also continuous without disruption, offering minimum transport resistance. Although the membranes discussed in previous studies [21, 27] are also reported to be *c*-oriented, their permeance values are much lower due to their disturbed straight

channels which result from a randomly oriented seed layer or miss-orientation of the channels after secondary growth.

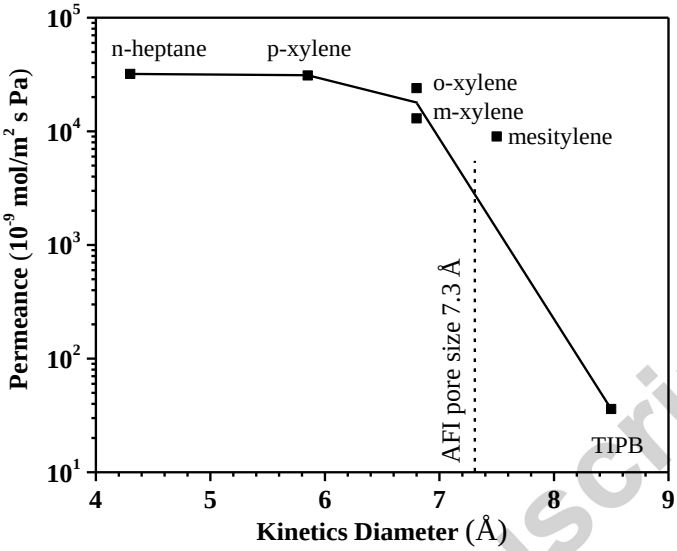

Fig. 9. Pervaporation permeance of hydrocarbon molecules with different sizes through the AFI membrane.

Table 1. Dimensions for various molecules in AFI channels

Molecules	*MW*	d_m (Å)[#]	σ_m (Å)*	d_m/d_c[§]	σ_m/d_c
He	4	2.60	2.98	0.36	0.41
H_2	2	2.89	3.14	0.40	0.43
CO_2	44	3.30	3.64	0.45	0.50
Ar	40	3.40	3.32	0.46	0.45
N_2	28	3.64	3.57	0.50	0.49
CH_4	16	3.80	3.71	0.52	0.53
C_2H_4	28	3.90	4.16	0.53	0.57
C_2H_6	30	4.00	4.33	0.55	0.59
C_3H_6	42	4.50	4.77	0.61	0.65
n-C_4H_{10}	58	4.30	5.42	0.59	0.74
i-C_4H_{10}	58	4.50	5.45	0.62	0.75
n-C_7H_{10}	94	4.30	6.07	0.59	0.83
p-C_8H_{10}	106	5.85	6.35	0.80	0.87
o-C_8H_{10}	106	6.80	6.30	0.93	0.86
m-C_8H_{10}	106	6.80	6.33	0.93	0.87
mesitylene	120	7.50	6.71	1.03	0.92
TIPB	204	8.50	8.75	1.16	1.20

[#]Kinetic diameter, obtained from Breck [40]
[*]Lennard-Jones length constant, estimated by Hirschfelder-Bird-Spotz method [41]
[§]d_c = 7.3 Å which is the diameter of AFI channel

3.5. Discussion of transport mechanism of gas molecules through AFI channels

The permeation mechanisms of guest molecules through microporous channels includes Knudsen diffusion, surface diffusion and molecular sieving, which depend on the pore size, guest molecular size and shape, interacting strength between the guest and the pore, and operation conditions. To reveal the physical parameters that affect the transport mechanism through AFI channels, we first adapt the normalized Knudsen-based permeance (NKP) method proposed by Tsuru and coworkers [42]. The NKP value of each diffusion species is defined as follows:

$$f_i = \frac{P_i}{P_{He}\sqrt{M_{He}/M_i}} \quad (4)$$

where P_i and M_i are the permeance and molecular weight of component i, respectively, and P_{He} and M_{He} are the permeance and molecular weight of helium, respectively. Here, although liquid pervaporation measurements were performed in a different way from gas permeation, its transportation driving force is the difference between permeate vapor pressure and vacuum pressure, which is similar to the pressure difference for gas permeation. Thus, it is reasonable to plot the gas permeance and liquid pervaporation permeance on one diagram. Fig. 10 shows the NKP values of all the studied diffusion species as a function of their kinetic diameter relative to the AFI pore size ratio, d_m/d_c. The kinetic diameters as well as the d_m/d_c values of all species studied in this work are listed in Table 1. For small molecules, when $d_m/d_c < 0.6$, the NKP value is approximately 1, indicating an activated Knudsen diffusion mechanism. When $0.6 < d_m/d_c < 1$, the NKP value jumps to almost 100, indicating that the diffusion mechanism has changed to surface diffusion. When $d_m/d_c > 1$, the NKP value drops to almost zero due to a strong molecular sieving effect.

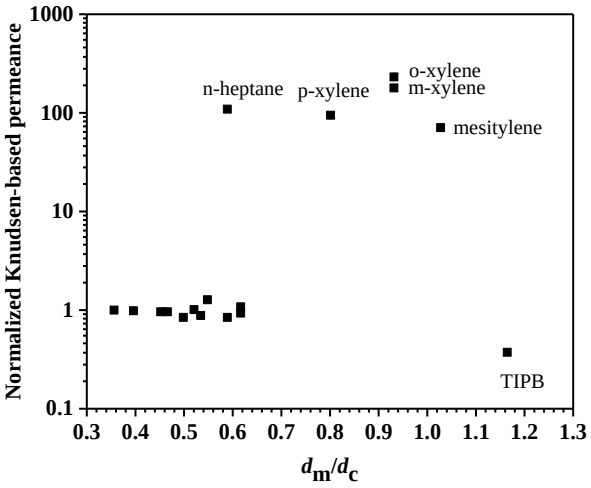

Fig. 10. Normalized Knudsen-based permeance as a function of d_m/d_c.

The above relationship between the transport mechanism and d_m/d_c matches very well the observations made for the ZSM-5 system by Xiao and Wei [34, 35]. In their studies, Xiao and Wei used two parameters, d_m/d_c and σ_m/d_m, to describe the transport behaviors, in which d_m/d_c was used to represent the molecular sieving effect, while σ_m/d_m was used to account for the effect of both molecular sieving and surface diffusion. σ_m is the Lennard-Jones parameter and it represents another molecular size in terms of the molecular interaction strength. Using a 10-4 Lennard Jones (L-J) potential, Everett and Powl [43] applied the ratio of σ_m/d_c to describe the adsorption potential evolution of a gas molecule in nanopores. Unlike the traditional 12-6 potential describing the interaction between a single atomic or molecular species, the 10-4 LJ potential describes the interaction between a single solid lattice plane (SLP) of 2 with a single molecule of 1 in the gas phase, as given by:

$$\varepsilon_{1,SLP} = 4\pi n r_0^2 \varepsilon_{12}^* \left[\frac{1}{5}\left(\frac{r_0}{z}\right)^{10} - \frac{1}{2}\left(\frac{r_0}{z}\right)^{4}\right] \quad (5)$$

where $\varepsilon_{1,SLP}$ is the potential energy inside the channel, n is the number of interacting centers per unit area of the lattice plane, ε_{12}^* is the depth of the potential energy minimum, $r_0 = \sigma^{1/2}$ is the

distance at which ε_{12} = 0, z is the distance from the plane of surface nuclei to the point. This equation can also be rewritten as:

$$\varepsilon_{1,SLP} = \frac{10}{3}\varepsilon^*_{1,SLP}\left[\frac{1}{5}\left(\frac{r_0}{z}\right)^{10} - \frac{1}{2}\left(\frac{r_0}{z}\right)^{4}\right] \quad (6)$$

where $\varepsilon^*_{1,SLP} = \frac{6}{5}\pi n\varepsilon^*_{12}r_0^2$ is the depth of the energy minimum occurring at a distance z* = r_0.

The potential equation corresponding to a long cylinder whose wall comprises a single layer of solid atoms can be derived from equations 5 and 6 and is expressed as follows:

$$\left|\frac{\varepsilon_{O,SL}(0)}{\varepsilon^*_{1,SLP}}\right| = \frac{5\pi}{2}\left(\frac{r_0}{R}\right)^{4}\left[1 - \frac{21}{32}\left(\frac{r_0}{R}\right)^{6}\right] \quad (7)$$

where R denotes the radius of the cylinder. Detailed descriptions of the above equations can be found in the literature [43, 44].

Fig. 11 illustrates the 10-4 Lennard Jones (L-J) adsorption potential in AFI channels at different σ_m/d_c ratios. The value of σ_m is estimated by the Hirschfelder-Bird-Spotz method [41], which is listed in Table 1 for each molecule. At small σ_m/d_c ratios, the interaction potential between the guest molecules and the wall exhibits a double minimum near the wall and a value close to free surface at the center, which means that only near the surface will guest molecules have strong interactions with the wall, while at the center they perform like free molecules. Hence, it is expected that Knudsen diffusion will play a dominant role. When the ratio of σ_m/d_c increases, the two minimums overlap with each other and eventually form a single minimum within the channel. The guest molecule is then restricted at the center of the channel and appears as *floating*. When σ_m/d_c = 0.93, the potential at the center reaches the deepest minimum. After that, the minimum potential increases rapidly because of the repulsive force.

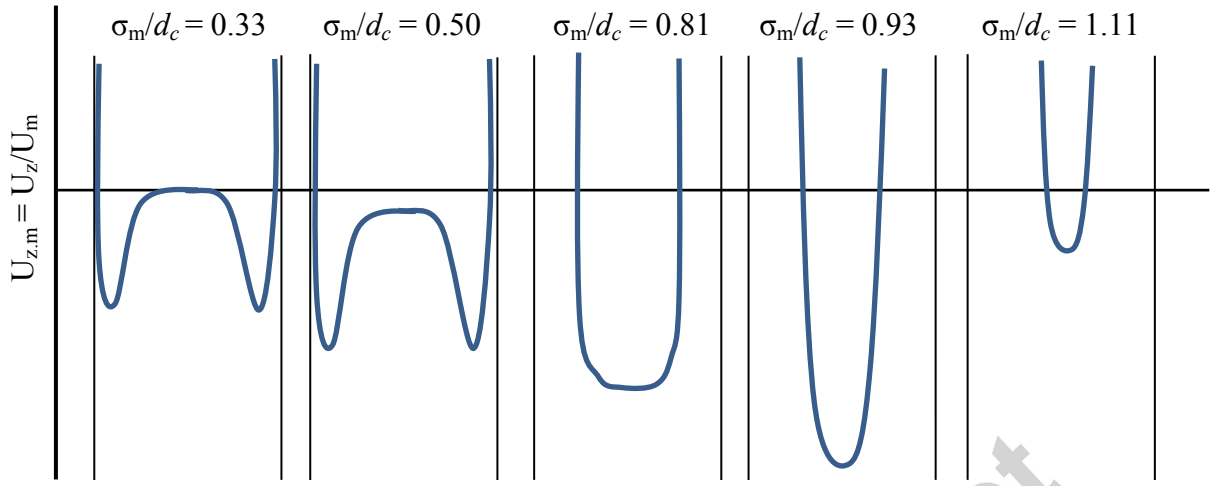

Fig. 11. The radial profile of the relative 10-4 L-J potential $U_{z,m} = U_z/U_m$ of the AFI channel at different σ_m/d_c ratios, where U_z is the absolute value of the L-J potential in the pore; U_m is L-J potential on a free surface; d_m is the kinetic diameter of the guest molecule; d_c is the diameter of the AFI channel.

Based on the physical meaning of σ_m, it appears that the ratio σ_m/d_c is a better parameter than the ratio, σ_m/d_m, in describing molecular transport. Hence, the normalized Knudsen-based permeance is plotted relative to the ratio of σ_m/d_c in Fig. 12. When $\sigma_m/d_c < 0.75$, diffusion is dominated by Knudsen diffusion. When $0.75 < \sigma_m/d_c < 1$, surface diffusion dominates and increases with the σ_m/d_c ratio. This is possibly attributed to the levitation effect that enhances the surface diffusion [45-47]. This occurs when the diameter of guest molecules approaches the pore diameter and thus the position of the interaction-energy potential minimum is located at the center of the channel: the molecules *float* at the center of the channels, an ideal situation to achieve supermobility [48, 49]. The σ_m/d_c ratio of mesitylene is approximately 0.92, which yields almost the strongest adsorption potential inside the channel, possibly explaining why it can transport fast through the AFI channels even though its kinetic diameter is slightly larger than the

AFI pore size. For TIPB, both d_m/d_c and σ_m/d_c are larger than 1, hence it is excluded from the channel due to both the molecular sieving effect and the repulsive force of the wall.

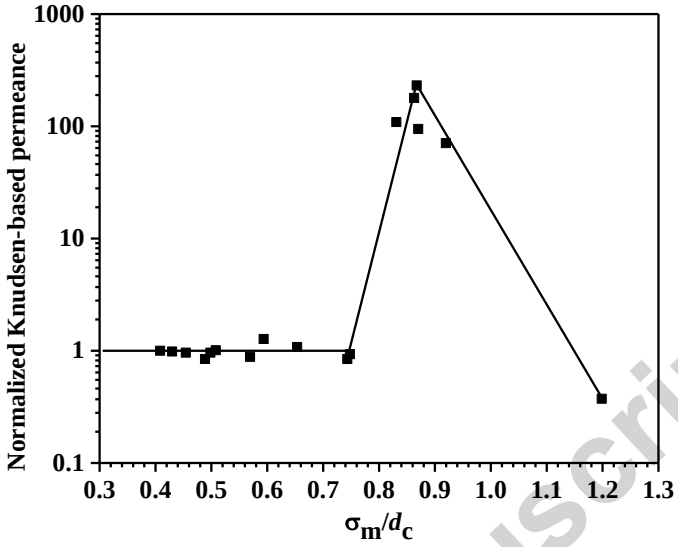

Fig. 12. Normalized Knudsen-based permeance as a function of σ_m/d_c.

4. Conclusions

Highly c-oriented and mechanically stable AFI type zeolite membranes were successfully fabricated on porous alumina supports using a secondary growth method. The procedure included synthesis of SAPO-5 seeds using fast microwave heating to obtain the desired plate-like morphology, assembly of the plate-like SAPO-5 seeds on a porous alumina support to form a c-oriented monolayer, and finally epitaxial growth of the seed layer through conventional hydrothermal synthesis to form a compact *c*-oriented film. Gas permeation and liquid hydrocarbon pervaporation studies revealed different transport mechanisms for different molecules. A clear molecular sieving effect was observed between hydrocarbons near the AFI pore size, which yielded a high selectivity of p-xylene to TIPB up to 850. The permeance values of the smaller hydrocarbons, such as n-heptane, xylene isomers and mesitylene, were almost two orders of magnitude higher than literature reported values. The high selectivity and high permeance indicate not only the compactness of the membrane but also the advantage of the

excellent membrane microstructure achieved by the novel seeded growth method; in other words, the straight channels in the membrane are not only aligned along the diffusion pathway but are also continuous, minimizing diffusion resistance. The highly c-oriented defect-free AFI membrane provides an ideal platform for experimentally investigating the diffusion behavior through straight uniform channels. Two parameters were found useful in explaining the transport behaviors: the ratio of kinetic diameter to channel diameter, d_m/d_c; and the ratio of the Lennard-Jones length constant to channel diameter, σ_m/d_c. When $d_m/d_c < 0.6$ or $\sigma_m/d_c < 0.75$, the diffusion is dominated by Knudsen diffusion; when $0.6 < d_m/d_c < 1$ or $0.75 < \sigma_m/d_c < 1$, surface diffusion dominates and it is enhanced as σ_m/d_c increases; when d_m/d_c and σ_m/d_c are both greater than 1, diffusion is blocked by molecular sieving. From the normalized permeance, it is found that the surface diffusion is almost two orders of magnitude faster than Knudsen diffusion, which is probably due to the levitation effect that enhances surface diffusion when the diameter of hydrocarbons approaches the channel size. The permeation studies have shown that the AFI membrane with a relatively simple porous structure is indeed a good platform for understanding the transport mechanism through nanopores. Hence, continuing work to investigate the effect of temperature, pressure and mixture composition are currently undergoing and will be reported in due course.

Acknowledgements

The work was funded by the KAUST competitive grant URF/1/1723.

References

[1] N. Kosinov, J. Gascon, F. Kapteijn, E.J.M. Hensen, Recent developments in zeolite membranes for gas separation, J. Membr. Sci., 499 (2016) 65-79.

[2] N. Rangnekar, N. Mittal, B. Elyassi, J. Caro, M. Tsapatsis, Zeolite membranes - a review and comparison with MOFs, Chem. Soc. Rev., 44 (2015) 7128-7154.

[3] S. Shirazian, S.N. Ashrafizadeh, LTA and ion-exchanged LTA zeolite membranes for dehydration of natural gas, J. Ind. Eng. Chem., 22 (2015) 132-137.

[4] S. Shirazian, S.N. Ashrafizadeh, Synthesis of substrate-modified LTA zeolite membranes for dehydration of natural gas, Fuel, 148 (2015) 112-119.

[5] F. Akhtar, E. Sjöberg, D. Korelskiy, M. Rayson, J. Hedlund, L. Bergström, Preparation of graded silicalite-1 substrates for all-zeolite membranes with excellent CO_2/H_2 separation performance, J. Membr. Sci., 493 (2015) 206-211.

[6] R. Zhou, H. Wang, B. Wang, X. Chen, S. Li, M. Yu, Defect-Patching of Zeolite Membranes by Surface Modification Using Siloxane Polymers for CO_2 Separation, Ind. Eng. Chem. Res., 54 (2015) 7516-7523.

[7] Z.P. Lai, G. Bonilla, I. Diaz, J.G. Nery, K. Sujaoti, M.A. Amat, E. Kokkoli, O. Terasaki, R.W. Thompson, M. Tsapatsis, D.G. Vlachos, Microstructural optimization of a zeolite membrane for organic vapor separation, Science, 300 (2003) 456-460.

[8] Z.P. Lai, M. Tsapatsis, Gas and Organic Vapor Permeation through b-Oriented MFI Membranes, Ind. Eng. Chem. Res., 43 (2004) 3000-3007.

[9] C. Baerlocher, W. Meier, D. Olson, Atlas of zeolite structure types, Elsevier, Amsterdam, (2001) 156.

[10] V. Kukla, J. Kornatowski, D. Demuth, I. Girnus, H. Pfeifer, L.V.C. Rees, S. Schunk, K.K. Unger, J. Kärger, NMR Studies of Single-File Diffusion in Unidimensional Channel Zeolites, Science, 272 (1996) 702-704.

[11] H.S. Kim, T.C. Pham, K.B. Yoon, A novel class of nonlinear optical materials based on host-guest composites: zeolites as inorganic crystalline hosts, Chem. Commun., 48 (2012) 4659-4673.

[12] F. Jiang, W. Lu, J. Zhai, J. Ye, G. Wong, J. Han, Z. Tang, Assembly of disperse red 1 molecules in the channels of $AlPO_4$-5 single crystals for second-harmonic generation, J. Phys. Chem. B, 110 (2006) 8924-8927.

[13] G. Calzaferri, R. Méallet‐Renault, D. Brühwiler, R. Pansu, I. Dolamic, T. Dienel, P. Adler, H. Li, A. Kunzmann, Designing Dye–Nanochannel Antenna Hybrid Materials for Light Harvesting, Transport and Trapping, ChemPhysChem, 12 (2011) 580-594.

[14] Z.K. Tang, L.Y. Zhang, N. Wang, X.X. Zhang, G.H. Wen, G.D. Li, J.N. Wang, C.T. Chan, P. Sheng, Superconductivity in 4 angstrom single-walled carbon nanotubes, Science, 292 (2001) 2462-2465.

[15] B. Bussemer, I. Dreiling, U.-W. Grummt, G.J. Mohr, Spectroscopic and quantum chemical study of the Brønsted acid sites in zeolite L channels with acidochromic cyanine dyes, J. Photochem. Photobiol., A 204 (2009) 90-96.

[16] L.J. Wang, C.W. Guo, S.R. Yan, X.D. Huang, Q.Z. Li, High-silica SAPO-5 with preferred orientation: synthesis, characterization and catalytic applications, Microp. Mesop. Mater., 64 (2003) 63-68.

[17] N. Kumar, J.I. Villegas, T. Salmi, D.Y. Murzin, T. Heikkila, Isomerization of n-butane to isobutane over Pt-SAPO-5, SAPO-5, Pt-H-mordenite and H-mordenite catalysts, Catal. Today, 100 (2005) 355-361.

[18] R. Roldan, M. Sanchez-Sanchez, G. Sankar, F.J. Romero-Salguero, C. Jimenez-Sanchidrian, Influence of pH and Si content on Si incorporation in SAPO-5 and their catalytic activity for isomerisation of n-heptane over Pt loaded catalysts, Microp. Mesop. Mater., 99 (2007) 288-298.

[19] N. Danilina, F. Krumeich, J.A. van Bokhoven, Hierarchical SAPO-5 catalysts active in acid-catalyzed reactions, J. Catal., 272 (2010) 37-43.

[20] N. Danilina, S.A. Castelanelli, E. Troussard, J.A. van Bokhoven, Influence of synthesis parameters on the catalytic activity of hierarchical SAPO-5 in space-demanding alkylation reactions, Catal. Today, 168 (2011) 80-85.

[21] C. Ji, Y. Tian, Y. Li, Y.S. Lin, Thin oriented AFI zeolite membranes for molecular sieving separation, Microp. Mesop. Mater., 186 (2014) 80-83.

[22] S.-E. Choi, H. Kim, Y.-S. Park, J.S. Lee, In-situ thickness controlled growth of $AlPO_4$-5 films, Microp. Mesop. Mater., 219 (2016) 155-160.

[23] I. Girnus, M.-M. Pohl, J. Richter-Mendau, M. Schneider, M. Noack, D. Venzke, J. Caro, Synthesis of $AlPO_4$-5 aluminumphosphate molecular sieve crystals for membrane applications by microwave heating, Adv. Mater., 7 (1995) 711-714.

[24] G.N. Karanikolos, J.W. Wydra, J.A. Stoeger, H. García, A. Corma, M. Tsapatsis, Continuousc-Oriented $AlPO_4$-5 Films by Tertiary Growth, Chem. Mater., 19 (2007) 792-797.

[25] W. Yang, B. Zhang, X. Liu, Synthesis and characterization of SAPO-5 membranes on porous α-Al_2O_3 substrates, Microp. Mesop. Mater., 117 (2009) 391-394.

[26] J.A. Stoeger, M. Palomino, K.V. Agrawal, X. Zhang, G.N. Karanikolos, S. Valencia, A. Corma, M. Tsapatsis, Oriented CoSAPO-5 membranes by microwave-enhanced growth on TiO_2-coated porous alumina, Angew. Chem. Int. Ed., 51 (2012) 2470-2473.

[27] E. Hu, Y.L.W. Huang, Q. Yan, D. Liu, Z. Lai, Synthesis of highly c-oriented AFI membranes by epitaxial growth, Microp. Mesop. Mater., 126 (2009) 81-86.

[28] G. Bonilla, D.G. Vlachos, M. Tsapatsis, Simulations and experiments on the growth and microstructure of zeolite MFI films and membranes made by secondary growth, Microp. Mesop. Mater., 42 (2001) 191-203.

[29] Z.P. Lai, M. Tsapatsis, J.F. Nicolich, Siliceous ZSM-5 Membranes by Secondary Growth of b-Oriented Seed Layers, Adv. Funct. Mater., 14 (2004) 716-729.

[30] S.H. Jhung, J.S. Chang, Y.K. Hwang, S.E. Park, Crystal morphology control of AFI type molecular sieves with microwave irradiation, J. Mater. Chem., 14 (2004) 280-285.

[31] A. Kulak, Y.S. Park, Y.-J. Lee, Y.S. Chun, K. Ha, K.B. Yoon, Polyamines as strong molecular linkers for monolayer assembly of zeolite crystals on flat and curved glass, J. Am. Chem. Soc., 122 (2000) 9308-9309.

[32] J.S. Lee, J.H. Kim, Y.J. Lee, N.C. Jeong, K.B. Yoon, Manual assembly of microcrystal monolayers on substrates, Angew. Chem. Int. Ed., 46 (2007) 3087-3090.

[33] A. Kasik, J. James, Y.S. Lin, Synthesis of ZIF-68 Membrane on a ZnO Modified α-Alumina Support by a Modified Reactive Seeding Method, Ind. Eng. Chem. Res., 55 (2016) 2831-2839.

[34] J. Xiao, J. Wei, Diffusion mechanism of hydrocarbons in zeolites—I. Theory, Chem. Eng. Sci., 47 (1992) 1123-1141.

[35] J. Xiao, J. Wei, Diffusion mechanism of hydrocarbons in zeolites—II. Analysis of experimental observations, Chem. Eng. Sci., 47 (1992) 1143-1159.

[36] D.H. Olson, M.A. Camblor, L.A. Villaescusa, G.H. Kuehl, Light hydrocarbon sorption properties of pure silica Si-CHA and ITQ-3 and high silica ZSM-58, Microp. Mesop. Mater., 67 (2004) 27-33.

[37] N. Zimmermann, S. Jakobtorweihen, E. Beerdsen, B. Smit, F. Keil, In-depth study of the influence of host-framework flexibility on the diffusion of small gas molecules in one-dimensional zeolitic pore systems, J. Phys. Chem. C, 111 (2007) 17370-17381.

[38] J.J. Gutiérrez‐Sevillano, S. Calero, S. Hamad, R. Grau‐Crespo, F. Rey, S. Valencia, M. Palomino, S.R. Balestra, A.R. Ruiz‐Salvador, Critical Role of Dynamic Flexibility in Ge‐Containing Zeolites: Impact on Diffusion, Chem. Eur. J., 22 (2016) 10036-10043.

[39] R. Krishna, J.M. van Baten, Comment on "modeling adsorption and self-diffusion of methane in LTA zeolites: the influence of framework flexibility", J. Phys. Chem. C, 114 (2010) 18017-18021.

[40] D.W. Breck, Zeolite molecular sieves: structure, chemistry, and use, Wiley, 1974.

[41] W. Volk, Applied statistics for engineers, McGraw-Hill, 1969.

[42] H.R. Lee, M. Kanezashi, Y. Shimomura, T. Yoshioka, T. Tsuru, Evaluation and fabrication of pore‐size‐tuned silica membranes with tetraethoxydimethyl disiloxane for gas separation, AIChE J., 57 (2011) 2755-2765.

[43] D.H. Everett, J.C. Powl, Adsorption in slit-like and cylindrical micropores in the henry's law region. A model for the microporosity of carbons, J. Chem. Soc., Faraday Trans., 72 (1976) 619-636.

[44] R. De Lange, K. Keizer, A. Burggraaf, Analysis and theory of gas transport in microporous sol-gel derived ceramic membranes, J. Membr. Sci., 104 (1995) 81-100.

[45] E.G. Derouane, J.-M. André, A.A. Lucas, A simple van der waals model for molecule-curved surface interactions in molecular-sized microporous solids, Chem. Phys. Lett., 137 (1987) 336-340.

[46] E.G. Derouane, J.-M. Andre, A.A. Lucas, Surface curvature effects in physisorption and catalysis by microporous solids and molecular sieves, J. Catal., 110 (1988) 58-73.

[47] S. Jakobtorweihen, F. Keil, B. Smit, Temperature and size effects on diffusion in carbon nanotubes, J. Phys. Chem. B, 110 (2006) 16332-16336.

[48] S.Y. Bhide, S. Yashonath, n-Pentane and isopentane in one-dimensional channels, J. Am. Chem. Soc., 125 (2003) 7425-7434.

[49] P.K. Ghorai, S. Yashonath, P. Demontis, G.B. Suffritti, Diffusion anomaly as a function of molecular length of linear molecules: Levitation effect, J. Am. Chem. Soc., 125 (2003) 7116-7123.

Highlights

(1) Highly c-oriented AFI membranes with continuous channels
(2) Order of magnitude improvement in pervaporation performance of hydrocarbons
(3) Detail studies of transport mechanisms through AFI channels